Mon. Not. R. Astron. Soc. **369,** 305–310 (2006) doi:10.1111/j.1365-2966.2006.10286.x

High-frequency quasi-periodic oscillations from GRS 1915+105 in its C state

T. Belloni,[1⋆] P. Soleri,[1,2,3] P. Casella,[1,3] M. Méndez[4] and S. Migliari[3,5]

[1]*INAF – Osservatorio Astronomico di Brera, Via E. Bianchi 46, I-23807 Merate (LC), Italy*
[2]*Università degli Studi di Milano, Dipartimento di Fisica, Via Celoria 16, 20133 Milano, Italy*
[3]*Astronomical Institute 'Anton Pannekoek', University of Amsterdam, and Center for High Energy Astrophysics, Kruislaan 403, 1098 SJ, Amsterdam, the Netherlands*
[4]*SRON, Netherlands Institute for Space Research, Sorbonnelaan 2, 3584 CA Utrecht, the Netherlands*
[5]*Center for Astrophysics and Space Sciences, Code 0424, University of California at San Diego, La Jolla, CA 92093, USA*

Accepted 2006 March 8. Received 2006 March 7; in original form 2006 February 8

ABSTRACT

We report the results of a systematic timing analysis of *RXTE* observations of GRS 1915+105 when the source was in its variability class θ, characterized by alternating soft and hard states on a time-scale of a few hundred seconds. The aim was to examine the high-frequency part of the power spectrum in order to confirm the hectohertz quasi-periodic oscillations (QPO) previously reported from observations from mixed variability behaviours. During the hard intervals (corresponding to state C in the classification of Belloni et al.), we find a significant QPO at a frequency of ∼170 Hz, although much broader (Q∼2) than previously reported. No other significant peak is observed at frequencies >30 Hz. A time-resolved spectral analysis of selected observations shows that the hard intervals from class θ show a stronger and steeper ($\Gamma = 2.8$–3.0) power-law component than hard intervals from other classes. We discuss these results in the framework of hectohertz QPOs reported from GRS 1915+105 and other black hole binaries.

Key words: accretion, accretion discs – X-rays: binaries.

1 INTRODUCTION

Since the launch of the NASA satellite *Rossi X-Ray Timing Explorer* (*RXTE*) in 1995, a number of high-frequency quasi-periodic oscillations (HFQPOs) have been discovered in several low-mass X-ray binaries (van der Klis 2006). Although many different theories have been formulated in the last decade (for a review, see van der Klis 2006), using different approaches in order to explain the observed phenomenology, no consensus has been reached at present on the physical origin of these features, and the work is still in progress in order to improve our knowledge of their behaviour.

In particular, HFQPOs have been discovered only in a few black hole candidates (BHCs). They often appear as transient and subtle features in the Fourier power density spectra (PDS), with centroid frequencies of tens to hundreds of Hz and low rms amplitude values (∼1–3 per cent) strongly dependent on the energy range (see e.g. Morgan, Remillard & Greiner 1997). Three BHCs show a single HFQPO: XTE J1650−500 (250 Hz; Homan et al. 2003), 4U 1630−47 (variable centroid frequency; Klein-Wolt, Homan & van der Klis 2004) and XTE J1859+226 (90 Hz; Cui et al. 2000), while other four sources exhibit pairs of HFQPOs: GRO J1655−40 (300 and 450 Hz; Remillard et al. 1999; Strohmayer 2001a), XTE J1550−564 (184 and 276 Hz; Homan et al. 2001; Miller et al. 2001; Remillard et al. 2002a), H1743−322 (165 and 241 Hz; Homan et al. 2005) and GRS 1915+105 (41 and 69 Hz; Morgan et al. 1997; Strohmayer 2001b). In many systems, the observed centroid frequencies appear rather stable, showing only small variations between different observations. As first noted by Abramowicz & Kluzniak (2001) for the case of GRO J1655−40, when two QPOs are observed, they appear at frequencies consistent with a simple ratio (2:3 or 3:5). As mentioned above, these features in the power spectra are very weak and observed only in a few cases. The relation between the detection of HFQPOs and source states is not completely clear, although it appears that most of them are observed during the soft intermediate state (see Belloni et al. 2005; Homan & Belloni 2005). At any rate, most of the QPO detections listed above are from observations when no type-C low-frequency QPOs are observed (see Casella, Belloni & Stella 2005, and references therein for a definition of these QPO types).

GRS 1915+105 is a very bright BHC that appeared in the X-ray sky in 1992 (Castro-Tirado, Brandt & Lund 1992) and has been bright in the sky ever since (see Fender & Belloni 2004, for a review). It is a very peculiar source which shows strong variability on time-scales of seconds to months, unique to this system (see Belloni et al. 2000). The first HFQPO detected in this system was at a

⋆E-mail: belloni@merate.mi.astro.it

frequency of ∼69 Hz and was observed in very few *RXTE* observations in 1996 (Morgan et al. 1997). The QPO has a hard energy spectrum, with an integrated fractional rms that increased from 1.5 per cent below 5 keV up to 6 per cent above 13 keV. The QPO appeared during observations where strong QPOs with a period of 15–20 s were observed. From the light curve and the hardness–intensity diagrams, it can be concluded that during these observations GRS 1915+105 was in its γ variability mode (see Belloni et al. 2000; Belloni, Méndez & Sánchez-Fernández 2001). Two of these observations were reanalysed by Belloni et al. (2001), who found that in one observation (1996 May 5) the 65-Hz QPO changed properties as a function of the phase of the ∼15 s oscillation, while in the other observation (1996 May 14), no significant 65-Hz QPO, but a 27-Hz QPO was visible at certain phases of the ∼15 s oscillation. A second QPO peak at a frequency of ∼41 Hz was detected by Strohmayer (2001b) by analysing *RXTE* data above 13 keV; unlike the 27-Hz one, this QPO was also detected simultaneously with a 67-Hz peak. It is interesting to note that 27:41:67 are in 2:3:5 ratio.

Remillard et al. (2002b) reported the detection of two additional HFQPO peaks from GRS 1915+105, at a frequency of 164 and 328 Hz, with the second one being consistent with the second harmonic of the first. These peaks were obtained from a selection in X-ray hardness and intensity in a set of *RXTE* observations from 1997 September. The selected parts of the observations were all from the C state of GRS 1915+105 (see Belloni et al. 2000), corresponding to the hard intermediate state (HIMS) in other transients (see Belloni et al. 2005; Homan & Belloni 2005). In this state, C-type QPOs are always observed and indeed are apparent in the power spectra from Remillard et al. (2002b). These detections are the only case of harmonically related HFQPOs and one of the rare cases of simultaneous presence of HFQPOs and type-C QPOs. Assuming they are different from the 27-, 41- and 69-Hz peaks (as they appear in different states, this is not at all guaranteed), this source would show at least four independent HFQPOs, three of them appearing in 2:3:5 ratio, and two higher frequency ones appearing in 1:2 ratio.

The work presented in this paper is aimed at searching for high-frequency QPOs in GRS 1915+105 following a procedure similar to that of Remillard et al. (2002b), extending the search to a broader data set, in order to better constrain their phenomenology. Many observations in the sample by Remillard et al. (2002b) belong to variability class θ (see Belloni et al. 2000). This class is characterized by alternating intervals of the soft state A and the harder state C; it is particularly interesting to note that the C-state intervals appear to be peculiar compared to other variability classes, being characterized by a rather high count rate and low values of X-ray hardness (see Belloni et al. 2000). We selected all available *RXTE* observations in the time interval 1996 April to 1999 March from the public archive which could be classified as class θ and performed a search for HFQPOs similar to that from Remillard et al. (2002b).

2 CLASS θ: COLOURS AND SPECTRA

Variability class θ as defined in Belloni et al. (2000) includes the only observations when the source does not go through state B. A typical *RXTE*/Proportional Counter Array (PCA) light curve (2–13 keV) is shown in the top panel of Fig. 1: the characteristic 'M' shape is caused by the alternating C-state (high rate and variable) and A-state (low rate and quiet) intervals. The corresponding colour–colour diagram, defined as in Belloni et al. (2000), is shown in the bottom left-hand panel of Fig. 1. State C corresponds to the cloud of points centred around (0.15, 1.0), while state A is represented by the soft points in the lower left-hand panel of the diagram.

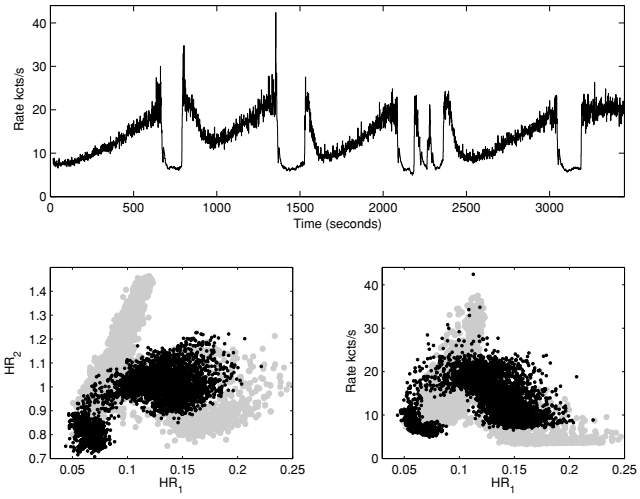

Figure 1. Top panel: PCA 2–13 keV θ light curve of GRS 1915+105 from 1997 September 5. Bottom panels: corresponding colour–colour diagram and hardness–intensity diagram (see Belloni et al. 2000). The grey points are from an observation of 1997 September 9, when the source was in its β class. The time resolution of all plots is one second.

As comparison, we plot in light grey also the points corresponding to a typical observation of class β. One can see that, in addition to the lack of the characteristic 'finger' going to state B, the state-C points of class θ are displaced with respect to class β. The differences can be clearly seen in the hardness–intensity diagram (see Belloni et al. 2000) shown in the bottom right-hand panel of Fig. 1. Note in particular how the θ points corresponding to state C have a much higher rate than those of class β. This class shows distinctive characteristics and has not been analysed as deeply as, for instance, class β (see e.g. Mirabel et al. 1998; Markwardt, Swank & Taam 1999; Migliari & Belloni 2003). Note that the θ and β observations shown in Fig. 1 are separated only by four days, indicating that the source can transit rather easily between these two 'modes'.

In order to examine the possible nature of these differences in the spectral domain, we applied to the PCA data of the observation of 1997 September 5 the same procedure for time-resolved spectral extraction described in Migliari & Belloni (2003). The energy spectra, with a 16-s time resolution, were fitted with a simple model consisting of the superposition of a disc blackbody (Mitsuda et al. 1984) and a power law. The interstellar absorption was fixed to 7×10^{22} cm^{-2}. The results for a full A-C-A cycle are shown in Figs 2 and 3 (in the same format as the corresponding figures for β observations in Migliari & Belloni 2003). Clear differences with the β case are evident: the disc component is fainter, and in state C the energy spectrum is dominated by a steeper power-law component. Note that this means that the observed count rate in the C-state interval is dominated by the power law more than the power-law flux indicates, given its spectral steepness.

In summary, the major peculiarities of this variability class are the absence of a state B and the strength and softness of the power-law component during state C.

3 TIMING/HARDNESS ANALYSIS

We examined all PCA light curves (with 1-s binning) of *RXTE* observations of GRS 1915+105 corresponding to PCA Gain Epoch 3 (1996 April 15 to 1999 March 22). For our analysis, we follow a procedure similar to that adopted by Remillard et al. (2002b).

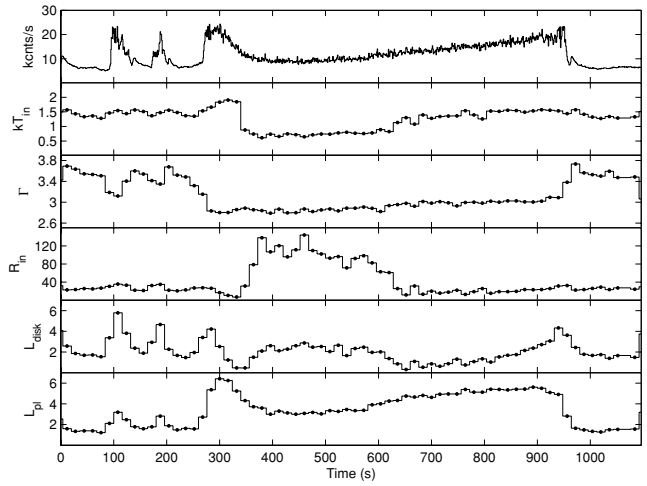

Figure 2. Panels from top to bottom: (1) PCA count rate (kcnts/s, 1-s bin size); (2) inner disc temperature (keV); (3) power-law photon index; (4) inner disc radius (km); (5) bolometric disc luminosity (10^{38} erg s^{-1}); (6) 3–25 keV power-law luminosity (10^{38} erg s^{-1}). See Migliari & Belloni (2003), for more details.

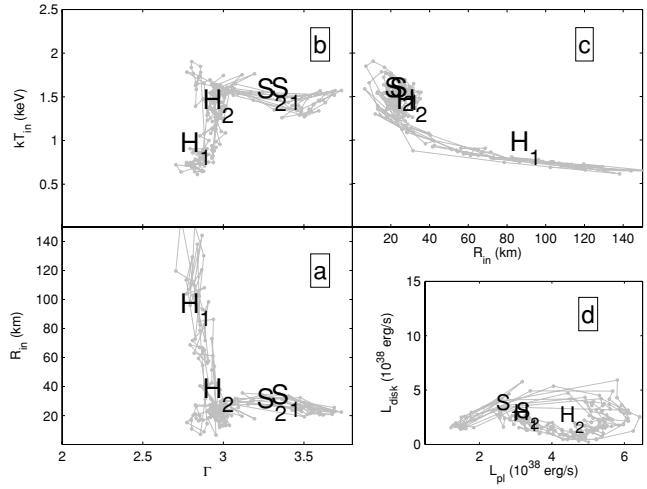

Figure 3. Correlations between the spectral parameters of Fig. 2. The axes have the same limits as Fig. 3 in Migliari & Belloni (2003), with the exception of the power-law luminosity, which in this case exceeds that limit. The H_n and S_n labels indicate average values corresponding to the rate-hardness selection in Section 3.1.

We divide each observation in intervals 16-s long. For each interval, we compute a total count rate from all proportional counter units (PCUs) in the Pulse Height Analyzer (PHA) channel range 0–79 (corresponding to 2–30 keV) and a hardness ratio defined as the ratio of counts in channel range 36–79 (13–30 keV) to those in channel range 0–35 (2–13 keV). As the source is very strong, we apply only an average background subtraction using fixed values for all the bands: this procedure does not modify significantly the shape of the hardness–intensity diagram. For each interval, we also compute a power spectrum from the 36–79 channel range (13–30 keV) covering the frequencies 0.0625–1024 Hz, which we normalize to square fractional rms (see Belloni & Hasinger 1990). As a precise estimate of the noise level due to Poissonian statistics is difficult to make, especially for such a strong source, and as the detection of high-frequency features depends crucially on this estimate, we do not subtracted the Poissonian level, but included it in our model as an additive constant value that is free to vary.

Table 1. The two groups of selected θ observations. # indicates the orbit number.

Obs. ID	Start date
10408-01-15-05	1996 June 16 14:23
10408-01-15-04	1996 June 16 15:59
10408-01-15-00	1996 June 16 17:35
10408-01-15-01	1996 June 16 19:11
10408-01-15-02	1996 June 16 20:47
10408-01-15-03	1996 June 16 22:23
10408-01-16-00	1996 June 19 14:25
10408-01-16-01	1996 June 19 16:01
10408-01-16-02	1996 June 19 17:37
10408-01-16-03	1996 June 19 19:13
10408-01-16-04 (#2)	1996 June 19 20:49
20402-01-45-02	1997 September 05 4:50
20186-03-02-00	1997 September 15 4:21
20186-03-02-01	1997 September 15 18:48
20186-03-02-02	1997 September 16 2:34
20186-03-02-03	1997 September 16 8:18
20186-03-02-04 (# 1, 2, 3)	1997 September 16 18:46
20187-02-04-00 (# 2)	1997 October 05 8:15

3.1 Analysis of class θ observations

As this variability class is characterized by a very clear pattern, we selected all observations which belonged to this class. The list of observations is shown in Table 1.

In Fig. 4, we show the total hardness–intensity diagram, as obtained from the complete data set in Table 1. The total number of points (with 16-s exposure) is 5741. We use the same time resolution, energy ranges and normalization to PCU2 adopted by Remillard et al. (2002b). Two main regions can be seen in the plot: the region at higher hardness corresponds to state C, while the smaller region at lower count rate and hardness corresponds to

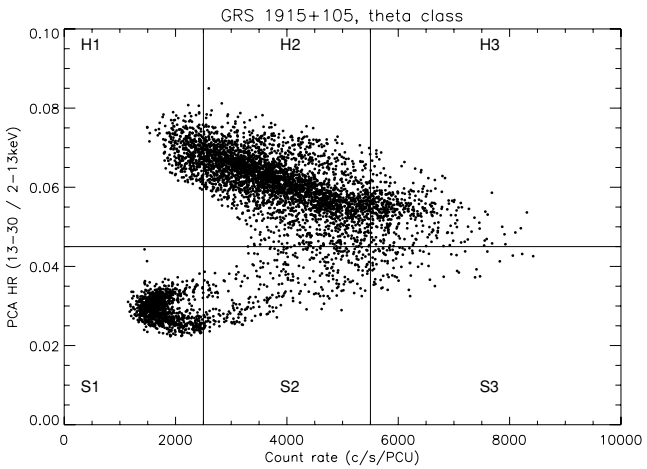

Figure 4. Hardness–intensity diagram for GRS 1915+105 using the *RXTE*/PCA observations for variability class θ listed in Table 1. Each point corresponds to an accumulation time of 16 s. The hardness (HR) is obtained as the ratio of source counts in the 13–30 keV band over those in the 2–13 keV band, while the intensity corresponds to 2–30 keV. The plot is divided into six regions according to the criteria of Remillard et al. (2002b).

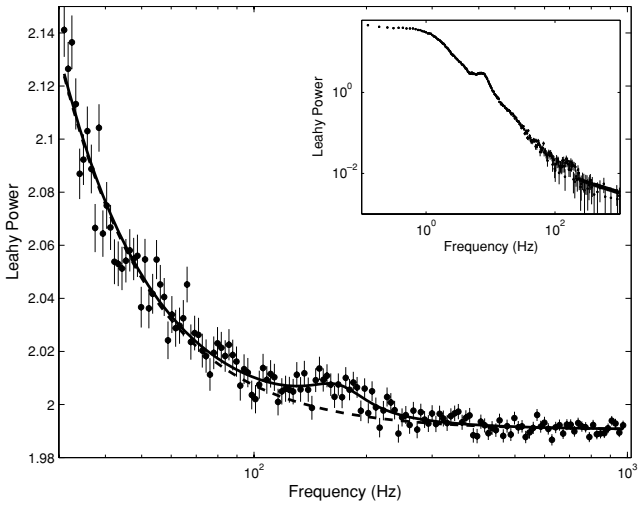

Figure 5. Power spectrum for the H2+H3 selection for the θ class observations (see Fig. 4). The main panel shows the high-frequency portion. The thick line represents the best-fitting model (see the text), while the dashed line is the same model with the Lorentzian component excluded. The inset shows the full power spectrum, after subtraction of the best-fitting Poissonian level.

state A. As expected, for these observations no state B is observed (see Belloni et al. 2000). The fast transitions between states A and C are represented mostly by the points in region S2 (see Fig. 4). Following Remillard et al. (2002b), we divided the Hardness–Intensity Diagram (HID) in six sections, marked in Fig. 4. In Fig. 3, we marked the position of the average spectral parameters corresponding to these regions (for S3 and H3, no points were present in this particular observation). We then averaged the power spectra for the two high-rate hard sections (H2 and H3) and for the union of the two sections (H2+H3). The number of points in the H2 and H3 regions are 3279 and 420, respectively, corresponding to an exposure of 52464 and 6720 s. The resulting power spectrum for H2+H3, limited to its high-frequency part (>30 Hz), is shown in Fig. 5.

We first fitted the three power spectra with a model consisting of a power law for the continuum noise and a flat component for the Poissonian component. We obtained reduced χ^2_ν values of 1.40, 1.14 and 1.33 for the regions H2, H3 and H2+H3, respectively.

A visual inspection of the residuals revealed the presence of a power excess around ∼160–180 Hz. We added a Lorentzian component in order to try to improve the fit by taking this excess into account and found a peak of significance between 3.8 and 4.3σ in H2 and H2+H3, respectively. Significances of detections are computed from the normalization of the Lorentzian components in power units. The results of these new fits are reported in Table 2.

For H2+H3 we have a 4.3σ detection; an F-test yields a probability of a chance improvement in the fit of less than 10^{-6}. The corresponding 166-Hz feature is broad, with a coherence factor

Table 2. Best-fitting parameters for the Lorentzian component for the θ observations. For H3, the quoted rms is a 3σ upper limit.

Region	Centroid (Hz)	FWHM (Hz)	rms (per cent)	χ^2_ν	Significance (# σ)
H2	164^{+7}_{-12}	91^{+37}_{-24}	3.9±0.5	1.08	3.8
H3	165 (FIX)	87.5 (FIX)	<1.1	1.07	–
H2H3	166±7	84^{+32}_{-20}	3.7±0.4	1.09	4.3

Table 3. Observations analysed by Remillard et al. (2002b).

Obs. ID	Start date	Class
20402-01-45-02	1997 September 5 4:50	θ
20402-01-45-00	1997 September 7 15:25	β
20402-01-45-01	1997 September 7 22:05	β
20402-01-45-03	1997 September 9 5:47	β
20402-01-46-00	1997 September 11 9:45	β
20186-03-02-00	1997 September 15 4:21	θ
20186-03-02-01	1997 September 15 18:48	θ
20186-03-02-02	1997 September 16 2:34	θ
20186-03-02-03	1997 September 16 8:18	θ
20186-03-02-04	1997 September 16 18:46	θ
20186-03-02-05	1997 September 17 1:09	χ_4
20186-03-02-06	1997 September 18 2:40	χ_4
20402-01-47-01	1997 September 19 0:00	χ_4
20402-01-48-00	1997 September 29 14:01	χ_4

$Q = \nu_c/\Delta = 2.0^{+0.5}_{-0.8}$, where ν_c is the centroid frequency and Δ is the full width at half-maximum (FWHM). For H3, we fixed centroid and width to an average between the H2 and H2+H3 detections and obtained a 3σ upper limit to the rms of 1.1 per cent (see Table 2). Similarly, we obtain a 3σ upper limit of 0.8 per cent for region H1.

3.2 The 1997 September observations

In order to compare our results with those presented by Remillard et al. (2002b), we analysed all the 14 *RXTE*/PCA observations made in the time interval 1997 September 5–29, corresponding to those selected and analysed by Remillard et al. (2002b) (see Table 3, for a log of these observations and for an identification of the class of variability according to Belloni et al. 2000). From Table 3, it is evident that this selection includes observations corresponding to different variability classes.

In Fig. 6, we show the total hardness–intensity diagram, as obtained from the complete data set. Note the difference with Fig. 4: the larger scatter of the points in this figure is caused by the mix of observations belonging to different variability classes. We used the same time resolution, energy ranges and normalization to PCU2

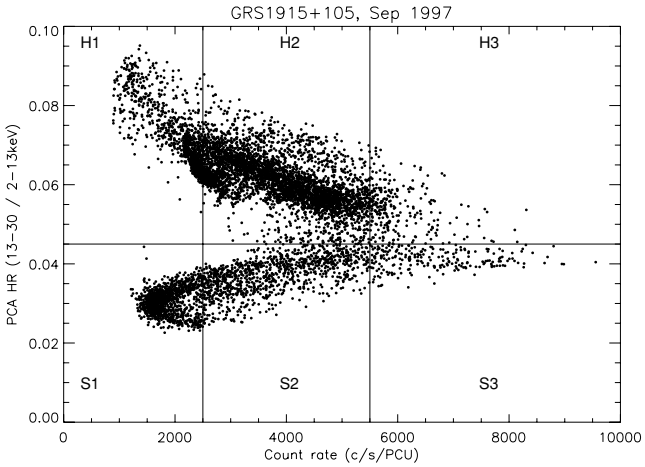

Figure 6. Hardness–intensity diagram for GRS 1915+105 using *RXTE*/PCA observations on 10 d during 1997 September 5–29. The parameters used to produce the diagram are the same as in Fig. 4. The plot is divided into six regions according to Remillard et al. (2002b).

Table 4. Best-fitting parameters for the Lorentzian component for the 1997 data set (Section 3.2). For H3, the quoted rms is a 3σ upper limit.

Region	Centroid (Hz)	FWHM (Hz)	rms (per cent)	χ^2_ν	Significance (# σ)
H2	166±8	60^{+28}_{-18}	2.8±0.5	1.08	2.97
H3	167 (FIX)	70 (FIX)	<1.0	1.04	–
H2H3	168^{+7}_{-11}	80^{+102}_{-27}	3.5±0.5	1.23	3.22

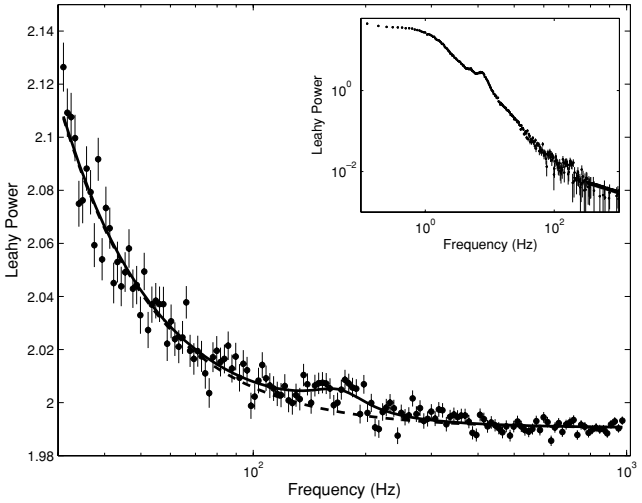

Figure 7. Power spectrum for the H2+H3 selection for the 1997 observations. The main panel shows the high-frequency portion. The thick line represents the best-fitting model (see the text), while the dashed line is the same model with the Lorentzian component excluded. The inset shows the full power spectrum, after subtraction of the best-fitting Poissonian level.

as before. We did not subtract the background contribution to the points: this is a negligible effect on the total count rate, while resulting only in a slight upward shift of the points due to the increase of hardness. As we did in the previous section, we divided the HID in six sections, and we averaged the power spectra for the two high-rate hard sections (H2 and H3) and for the union of the two sections (H2+H3).

As we did for the θ-class observation, we first fitted the high-frequency portions of these spectra (30–1000 Hz) with a simple power-law model (plus a constant for the Poissonian contribution). The reduced χ^2_ν values we obtained are 1.42, 1.07 and 1.50 for H2, H3 and H2+H3, respectively.

For H2 and H2+H3, where χ^2_ν was higher than unity, we then added a Lorentzian component to account for the residuals between 100 and 200 Hz and obtained the best fits shown in Table 4. The power spectrum corresponding to H2+H3 is shown in Fig. 7. For H3, we fixed centroid and width to an average between the H2 and H2+H3 detections and obtained a 3σ upper limit to the rms (see Table 4).

4 DISCUSSION

We investigated the presence of high-frequency QPOs in a particular class of observations of GRS 1915+105, class θ from Belloni et al. (2000), characterized by the presence of a steep hard component in the energy spectrum during state-C intervals. State C is the one where type-C QPOs are always observed (see Belloni et al. 2000). We find evidence for the presence of a broad peaked component modelled with a Lorentzian with centroid frequency $\nu_c = 166 \pm 7$ and FWHM $\Delta = 84^{+32}_{-20}$. In the 13–30 keV band, the integrated fractional rms of this component is 3.7 per cent. The quality factor $Q = 2.0^{+0.5}_{-0.8}$. Comparing our results with those of Remillard et al. (2002b), we confirm the presence of a feature around 170 Hz; however, our peak is stronger, as theirs had a fractional rms of 1.6 per cent in the same energy band, and our Q value is substantially lower (2 versus 5–7). Even using the same data set, we do not confirm the presence of significant peaks at higher frequencies. The reason of this discrepancy is unclear, although it could be related to the different technique to account for the Poissonian noise level, for which we took a more conservative approach. The difference in width cannot be attributed to the largest sample of observations analysed here, which could include more variations in frequency, as it is also found from the same sample used by Remillard et al. (2002b). The difference in fractional rms is probably directly related to the difference in width, since it is the integral of the Lorentzian function used for the fit. The difference in removal of the Poissonian contribution could have played a role as well.

To date, most high-frequency QPOs detected in BHCs were observed during states which excluded the presence of type-C QPOs. In this case, a clear type-C QPO is observed (see Figs 5 and 7), as it is normal for the state C of GRS 1915+105 (see Belloni et al. 2000). Interestingly, HFQPOs are detected together with type-C QPOs also in the 2005 outburst of GRO J1655–40 (Homan, private communication). These detections and the one reported here have in common the fact that in both cases the detection corresponds to the softest spectra associated with type-C QPOs (see Fig. 3). Therefore, although the mutual exclusion of type C and HFQPOs does not strictly hold, the latter are confirmed to be detected in correspondence of a small range in spectral parameters.

In summary, the confirmed detections of HFQPOs (with frequencies >20 Hz) in GRS 1915+105 to date are as follows.

(i) *27 Hz*: detected in one observation on 1996 March 14 (variability class γ) only in correspondence of the minima in the slow (period ∼15 s) oscillation (Belloni et al. 2001).

(ii) *41 Hz*: detected in a set of observations in the period 1997 July–November, all of variability class γ (Strohmayer 2001b).

(iii) *65–67 Hz*: detected in two observations from 1996 April 20 and May 5 (Morgan et al. 1997). The other detections from this period (Morgan et al. 1997) have significances well below 3σ (Belloni et al. 2001). Both observations belong to class variability γ. The strong 65.5-Hz QPO from May 5 shows very strong spectral changes with the ∼15 s slow oscillation (Belloni et al. 2001).

(iv) *69 Hz*: detected together with the 41-Hz QPO by Strohmayer (2001b) in the 1997 γ-class observations. Although their frequency is not formally compatible with 65–67 Hz, this QPO is most likely the same as the ones found by Morgan et al. (1997).

(v) *166 Hz*: detected by Remillard et al. (2002b) and confirmed in this work through a more homogeneous and complete selection of observations. It is observed in the average of a rather large number of observations from 1996 June to 1997 October. All these observations are of variability class θ, at variance with the previous ones, which were all of class γ. We do not find significant peaks at higher frequencies. As shown before, unlike the previous ones, this feature is rather broad.

To date there is no record of a 113-Hz oscillation as reported by McClintock & Remillard (2006). Identifying the 65–67 Hz oscillations with the 69-Hz one, we have *four* different characteristic frequencies. The only ones that were ever observed at the same time

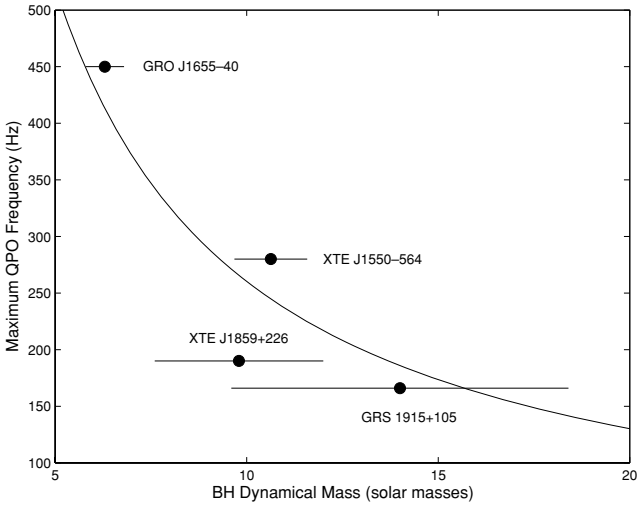

Figure 8. Plot of the highest QPO frequency observed versus dynamical black hole mass for black hole systems for which both HFQPOs and a mass estimate are available. The line is the best fit with a 1/M law.

were the 41 and 69 Hz, while the others seem to be mutually exclusive. The values 27:41:69 are roughly in ratio 2:3:5, while in this sequence the 166-Hz peak would be at 12.3.

In order to compare the frequencies observed in the different systems with the dynamical masses for the black hole one needs to follow a rigid criterion for the choice of the peaks. In the absence of other indications, the obvious choice would be to consider the highest observed frequency for each system. We can therefore plot these frequencies as a function of the black hole mass for GRO J1655−40, XTE J1550−546, GRS 1915+105 and XTE J1859+226 (masses from McClintock & Remillard 2005; the other two systems with high-frequency QPOs, H 1743−322 and XTE J1650−500, do not have a dynamical estimate for the mass of the black hole). The resulting plot can be seen in Fig. 8, where we also plot the best-fitting 1/M relation. Although the fits are by no means good, the general trend is the expected one.

The QPO reported here is observed in the C state of GRS 1915+105, which corresponds to the HIMS of other black hole transients (see Fender & Belloni 2004; Belloni et al. 2005; Homan & Belloni 2005). Most models for the production of these oscillations associate the highest-frequency peak with the Keplerian time-scale at the innermost stable orbit around the black hole. Recently, multiwavelength observations of GX 339−4 in its hard state indicated that the thermal accretion disc was not truncated (Miller et al. 2006). From Fig. 3, we can see that region H2 corresponds to an inner disc radius already at its minimum value, when a bright disc component is observed at all times, although it is not the dominating one. At any rate, HFQPOs have a hard spectrum, being observed at high energies (see Morgan et al. 1997) where the contribution of the thermal disc component is negligible. Therefore, no direct association should be made with the thermal component. Interestingly, this is the highest frequency observed in GRS 1915+105 and it corresponds to a harder energy spectrum than that associated with the other detections. This seems to exclude an inverse relation between hardness and QPO frequency.

Finally, we note that all detections of narrow ($Q \geqslant 2$) high-frequency features from BHCs are observed when a thermal disc component is present in the energy spectrum, together with a rather steep hard component. No such detection corresponds to the high/soft state, where the hard component is very weak, nor to the low/hard state, where the hard component is flat and the disc component is weak or absent in the PCA energy band. All detections can be associated with intermediate states (see Homan & Belloni 2005). However, these features are so weak and elusive that from the observations it is not clear what precise conditions are associated with their presence.

REFERENCES

Abramowicz M., Kluzniak W., 2001, A&A, 2001, L19
Belloni T., Hasinger G., 1990, A&A, 230, 103
Belloni T., Klein-Wolt M., Méndez M., van der Klis M., van Paradijs J., 2000, A&A, 355, 271
Belloni T., Méndez M., Sánchez-Fernández C., 2001, A&A, 372, 551
Belloni T., Homan J., Casella P., van der Klis M., Nespoli E., Lewin W. H. G., Miller J. M., Méndez M., 2005, A&A, 440, 207
Casella P., Belloni T., Stella L., 2005, ApJ, 629, 403
Castro-Tirado A. J., Brandt S., Lund N., 1992, IAUC, 5590
Cui W., Shrader C. R., Haswell C. A., Hynes R. I., 2000, ApJ, 535, L123
Fender R. P., Belloni T., 2004, ARA&A, 42, 317
Homan J., Belloni T., 2005, Ap&SS, 300, 107
Homan J., Wijnands R., van der Klis M., Belloni T., van Paradijs J., Klein-Wolt M., Fender R. P., Méndez M., 2001, ApJS, 132, 377
Homan J., Klein-Wolt M., Rossi S., Miller J. M., Wijnands R., Belloni, T., van der Klis M., Lewin W. H. G., 2003, ApJ, 586, 1262
Homan J., Miller J. M., Wijnands R., van der Klis M., Belloni T., Steeghs D., Lewin W. H. G., 2005, ApJ, 623, 383
Klein-Wolt M., Homan J., van der Klis M., 2004, Nucl. Phys. B, 132, 381
Markwardt C. B., Swank J. H., Taam R. E., 1999, ApJ, 513, L37
McClintock J. E., Remillard R. A., 2006, in Lewin W. H. G., van der Klis M., eds, Compact Stellar X-Ray Sources. Cambridge Univ. Press, Cambridge
Migliari S., Belloni T., 2003, A&A, 404, 283
Miller J. M. et al., 2001, ApJ, 563, 928
Miller J. M., Homan J., Steeghs D., Rupen M., Hunstead R. W., Wijnands R., Charles P. A., Fabian A. C., 2006, ApJ, submitted, (astro-ph/0602633)
Mirabel I. F., Dhawan V., Chaty S., Rodríguez L. F., Martí J., Robinson C. R., Swank J. H., Geballe T. R., 1998, A&A, 330, L9
Mitsuda K. et al., 1984, PASJ, 36, 741
Morgan E. H., Remillard R. A., Greiner J., 1997, ApJ, 482, 993
Remillard R. A., McClintock J. E., Sobczak G. J., Bailyn C. D., Orosz J. A., Morgan E. H., Levine A. M., 1999, ApJ, 517, L127
Remillard R. A., Sobczak G. J., Muno M. P., McClintock J. E., 2002a, ApJ, 564, 962
Remillard R. A., Muno M., McClintock J., Orosz J., 2002b, in Durouchoux Ph., Fuchs Y., Rodriguez J., eds, New Views on Microquasars. Center for Space Physics, Kolkata, India, p. 49
Strohmayer T., 2001a, ApJ, 552, L49
Strohmayer T., 2001b, ApJ, 554, L169
van der Klis M., 2006, in Lewin W. H. G., van der Klis M., eds, Compact Stellar X-Ray Sources. Cambridge Univ. Press, Cambridge

This paper has been typeset from a TEX/LATEX file prepared by the author.